RESEARCH ARTICLE

Correspondence to:
J. Pisek,
janpisek@gmail.com

Retrieval of seasonal dynamics of forest understory reflectance from semiarid to boreal forests using MODIS BRDF data

Jan Pisek[1], Jing M. Chen[2], Hideki Kobayashi[3], Miina Rautiainen[4,5], Michael E. Schaepman[6], Arnon Karnieli[7], Michael Sprinstin[8], Youngryel Ryu[9], Maris Nikopensius[1], and Kairi Raabe[1]

[1]Tartu Observatory, Tõravere, Estonia, [2]Department of Geography and Program in Planning, University of Toronto, Toronto, Ontario, Canada, [3]Department of Environmental Geochemical Cycle Research, Japan Agency for Marine-Earth Science and Technology, Yokohama, Japan, [4]School of Engineering, Department of Built Environment, Aalto University, Aalto, Finland, [5]School of Electrical Engineering, Department of Radio Science and Engineering, Aalto University, Aalto, Finland, [6]Remote Sensing Laboratories, Department of Geography, University of Zurich, Zurich, Switzerland, [7]Remote Sensing Laboratory, Jacob Blaustein Institute for Desert Research, Ben Gurion University of the Negev, Be'er Sheva, Israel, [8]Forest Management and GIS Department, Jewish National Fund-Keren Kayemet Lelsrael, Jerusalem, Israel, [9]Department of Landscape Architecture and Rural Systems Engineering, Seoul National University, Seoul, South Korea

Abstract Spatial and temporal patterns of forest background (understory) reflectance are crucial for retrieving biophysical parameters of forest canopies (overstory) and subsequently for ecosystem modeling. In this communication, we retrieved seasonal courses of understory normalized difference vegetation index (NDVI) from multiangular Moderate Resolution Imaging Spectroradiometer bidirectional reflectance distribution function (MODIS BRDF)/albedo data. We compared satellite-based seasonal courses of understory NDVI to understory NDVI values measured in different types of forests distributed along a wide latitudinal gradient (65.12°N–31.35°N). Our results indicated that the retrieval method performs well particularly over open forests of different types. We also demonstrated the limitations of the method for closed canopies, where the understory signal retrieval is much attenuated.

1. Introduction

Ground vegetation (understory) is an important component of forest ecosystems typically supporting the majority of total ecosystem floristic diversity [*Gilliam and Roberts*, 2003; *D'Amato et al.*, 2009]. Understory plays a central role in the dynamics and functioning of forest ecosystems by influencing long-term successional patterns [*Hart and Chen*, 2006; *Nyland et al.*, 2006] and facilitates nutrient cycling and energy flow as ecosystem drivers [*Chapin*, 1983; *Chastain et al.*, 2006; *Nilsson and Wardle*, 2005].

The understory layer can go through versatile spectral changes during the growing period. The strength of the cycle depends on site fertility [*Rautiainen et al.*, 2011]. The understory might also differ in phenology and in response to the seasonal shifts of light intensity [*Koizumi and Oshima*, 1985; *Richardson and O'Keefe*, 2009]. Importantly, the understory layer provides an essential contribution to the whole-stand reflectance signal in many boreal, subboreal, and temperate forests. Accurate knowledge about forest understory reflectance is urgently needed in various forest reflectance modeling efforts [*Gemmell*, 2000; *Kobayashi et al.*, 2007; *Suzuki et al.*, 2011; *Lukeš et al.*, 2013; *Gonsamo and Chen*, 2014]. However, systematic collections of understory reflectance data covering different sites and ecosystems are almost missing.

Measurement of understory reflectance is a real challenge because of an extremely high variability of irradiance at the forest floor, weak signal in some parts of the spectrum, spectral separability issues of overstory and understory [*Schaepman et al.*, 2009], and its variable nature [*Miller et al.*, 1997]. Understory can consist of several sublayers (regenerated tree, shrub, grasses or dwarf shrub, mosses, lichens, litter, and bare soil) and has spatially temporally variable species composition and ground coverage. Additional challenges are introduced by patchiness of ground vegetation, ground surface roughness, and understory-overstory relations [*Peltoniemi et al.*, 2005; *Rautiainen and Heiskanen*, 2013]. Due to this variability, remote sensing might be the only means to provide consistent data at spatially relevant scales [*Pinty et al.*, 2008].

In this communication, we follow upon our previous effort at mapping understory reflectance dynamics using multiangle remote sensing observations [*Canisius and Chen*, 2007; *Pisek and Chen*, 2009; *Pisek et al.*, 2010, 2012,

2015a, 2015b; *Jiao et al.*, 2014]. Here we focus on the validation of those approaches using MODIS bidirectional reflectance distribution function (BRDF)/albedo data [*Schaaf et al.*, 2002] against an extended collection of different types of forest sites with available in situ understory reflectance measurements. These sites are distributed along a wide latitudinal gradient on the Northern Hemisphere: a sparse and dense black spruce forests in Alaska and Canada, a northern European boreal forest in Finland, hemiboreal needleleaf and deciduous stands in Estonia, a mixed temperate forest in Switzerland, a cool temperate deciduous broadleaf forest in Korea, and a semiarid pine plantation in Israel. The wide range of included different forest types allows us to better understand possibilities and limits of our method and its performance under various growing conditions. Specifically, we seek to answer the following questions:

1. Is it possible to track actual understory normalized difference vegetation index (NDVI) dynamics throughout the whole growing season using MODIS BRDF data?
2. Are there important differences in seasonal dynamics of understory NDVI between different sites?
3. Can we detect and track any differences between the seasonal dynamics of forest overstory and understory layers with this approach?
4. What are the limitations of the proposed retrieval method?

2. Materials

2.1. Study Sites

The study sites comprise different types of forest along a wide latitudinal gradient. Detailed site descriptions are provided in Table 1.

There are two North American boreal evergreen needleleaf stands: a sparse black spruce forest in Poker Flat Research Range, AL, USA (PFRR; 65.12°N, 147.5°W) and a dense black spruce forest near Sudbury, ON, Canada (47.16°N, 81.76°W). Both sites lack tall understory vegetation. The forest floor vegetation is dominated by low shrubs and herbs such as Labrador tea (*Ledum groenlandicum*), bog bilberry (*Vaccinium uliginosum*), dwarf birch (*Betula nana*), and cloudberry (*Rubus chamaemorus*) in PFRR [*Kobayashi et al.*, 2014]. The understory vegetation at Sudbury site consisted mainly of feather moss (*Hylocomium splendens*) with varying contributions from labrador tea (*Ledum groenlandicum*) and leather leaf (*Chamaedaphne calyculata*) [*Pisek et al.*, 2010].

A southern boreal zone in Europe is represented by two stands in Hyytiälä in central Finland. Dominant tree species are Scots pine (*Pinus sylvestris*) at the xeric heath forest (61.81°N, 24.33°E) and birches (*Betula pubescens* and *Betula pendula*) at the herb-rich site (61.84°N, 24.32°E). The growing season typically begins in early May and senescence in late August. The xeric heath forest understory is dominated by lichens and heather. The herb-rich heath forest understory is dominated by herbaceous species and graminoids. *Rautiainen et al.* [2011] provide more detail.

There are two different forest stands from the adjoining hemiboreal zone in Estonia. The Järvselja RAMI (Radiation Model Intercomparison) [*Widlowski et al.*, 2007] pine stand (58.31°N, 27.30°E) grows on a transitional bog. The understory vegetation is composed of sparse labrador tea (*Ledum palustre*), cotton grass (*Eriophorum vaginatum*), and a continuous *Sphagnum* ssp. moss layer. The RAMI birch stand (58.28°N, 27.33°E) can be described as an herb-rich forest, dominated by the herbaceous species and graminoids; moss layer is sparse or missing [*Nikopensius et al.*, 2015]. The understory vegetation, in general, is more abundant and hosts more species in hemiboreal Järvselja than in boreal Hyytiälä.

The CarboEurope forest flux site Laegern (47.48°N, 8.35°E) in Switzerland represents a temperate mixed forest. The overstory is dominated by European beech (*Fagus sylvatica*) and Norway spruce (*Picea abies*). The understory vegetation is rather scarce and consists mainly of *Allium ursinum* [*Eugster et al.*, 2007]. Overstory [*D'odorico et al.*, 2014] and understory [*Leiterer et al.*, 2015] vegetation behavior is characterized using a multitude of methods.

Gwangneung, a core site of KoFlux network, is a broadleaf stand in a cool temperate forest in Korea (37.75°N, 127.15°E). Overstory canopy consists of *Quercus acutissima*, *Quercus serrata*, and *Carpinus laxiflora*. Dominant understory species include *Euonymus oxyphyllus* and *Cornus kousa*. Both overstory and understory species are deciduous [*Ryu et al.*, 2014; *Song and Ryu*, 2015].

Yatir forest in Israel (31.35°N, 35.03°E) is a monoculture semiarid plantation dominated by Aleppo pine (*Pinus halepensis* Mill.) [*Maseyk et al.*, 2008]. Sparse understory vegetation develops only during the rainy season (November–March) [*Grünzweig et al.*, 2003].

Table 1. Study Site Descriptions[a]

Site Name	PFRR	Sudbury	Hyytiälä Xeric	Hyytiälä Herb Rich	Järvselja RAMI Pine	Järvselja RAMI Birch	Laegern	Gwangneung	Yatir
Location	AL, USA	ON, Canada	Finland	Finland	Estonia	Estonia	Switzerland	Korea	Israel
Latitude (deg)	65.12°N,	47.16°N,	61.81°N,	61.84°N,	58.31°N,	58.28°N,	47.48°N,	37.74°N,	31.35°N,
Longitude (deg)	147.5°W	81.76°W	24.33°E	24.32°E	27.30°E	27.33°E	8.35°E	127.14°E	35.03°E
Overstory	PM	PM	SP	SB	SP	BP, AG, PT	FS, PA	QA, QS, CL	PH
LAIe	0.62	2.08	1.5	3.5	1.75	2.94	1–5.5	3.6	1.74
Mean tree height (m)	2.4 + -1.1	15.9	16.6	14.9	16(1.5)	22(5.5)	30.6	18	10
Tree density (trees ha^{-1})	3978	4000	790	990	1122	992	1838	838	300
Crown radius (m)	0.4	0.5	n/a	n/a	1.86	2	2.8	n/a	2.3
Dominating understory species	*Vaccinium corymbosum*, moss, and lichen	*Hylocomium splendens, Ledum groenlandicum*, and *Chamaedaphne calyculata*	*Vaccinium vitis-idaea, Calluna vulgaris*, mosses, and lichens	*Vaccinium myrtillus, Vaccinium vitis-idaea, Deschampsia flexuosa*, and *Calamagrostis* spp	*Ledum palustre, Eriophorum vaginatum*, and continuous *Sphagnum* ssp.	*Anemone nemorosa, Oxalis acetosella, Agrostis Stolonifera*, and *Sphagnum* ssp.	sparse; *Allium ursinum* L.	*Euonymus oxyphyllus* and *Cornus kousa*	sparse grass
Reference	*Kobayashi et al.* [2014]	*Pisek et al.* [2010]	*Rautiainen et al.* [2011]	*Rautiainen et al.* [2011]	*Nikopensius et al.* [2015]	*Nikopensius et al.* [2015]	*Schneider et al.* [2014]	*Ryu et al.* [2014]	*Sprintsin et al.* [2011]

[a]PM, *Picea mariana*; PS, *Pinus sylvestris*; BP, *Betula pendula*; AG, *Alnus glutinosa*; PT, *Populus tremula*; FS, *Fagus sylvatica*; PA, *Picea abies*; QA, *Quercus acutissima*; QS, *Quercus serrata*; CL, *Carpinus laxiflora*; PH, Pinus halepensis; LAIe, estimates of LAI from ground measurements of gap (green) fraction for a specific configuration, assuming random distribution of the elements within the canopy volume (i.e., no clumping).

Table 2. Understory Spectra Measurement Descriptions

Site	PFRR	Sudbury	Hyytiälä	Järvselja	Laegern	Gwangneung	Yatir
Year/month	2010/6	2007/6	2010/5–9	2013/5–9	2011/9	2013/3–12	2015/2
Spectrometer model	MS-720	ASD FieldSpec Pro	ASD FieldSpec Pro	ASD FieldSpec Pro	ASD FieldSpec Pro	LED (SMF-HM153 0SRD-509;QED223)	ASD FieldSpec Pro
Field of view	25°	25°	25°	25°	25°	180°	25°
Diameter of measured area (m)	-	0.025	0.5	0.5	-		0.5
Spectral range (nm)	350–1050	350–1050	325–1075	350–1050	354–2450	618-674; 807-879	350–1050
Spectral resolution (nm)	3 nm	3 nm	3.5 nm	3 nm	3 nm	-	3 nm
Illumination conditions	clear sky	clear sky	diffuse	diffuse	clear sky	diffuse	diffuse
Sampling	various floor conditions	individual components	every 0.7 m along 28 m transect	every 2 m along 100 m transect	individual components	sensors installed on tower	every 2 m along 100 m transect

2.2. In Situ Measurements

In this work the reflectance factors measured by the field spectrometers are referred similarly to the satellite-derived hemispherical-directional reflectance factors (HDRFs, terminology following *Schaepman-Strub et al.* [2006]). We approximate the field of view of the ground spectrometers to be angular, and some anisotropy was captured corresponding to normal remote sensing viewing geometry. Overview of individual in situ campaigns is provided in Table 2.

At PFRR, spectral HDRFs of the black spruce forest floor were measured in July 2010 under clear skies. *Kobayashi et al.* [2014] used a spectrometer (MS-720, EKO, Inc.) that measures from 350 to 1050 nm with a 3 nm spectral resolution. The measured spectral HDRFs were weighted for incoming spectral solar fluxes.

The sunlit reflectance of the present forest floor types at Sudbury was reported by *Pisek et al.* [2010] using a FieldSpec Pro spectrometer (ASD, Analytical Spectral Devices, Inc., Boulder, CO, USA). *Pisek et al.* [2010] took several sets of spectral reflectance measurements at different locations within the forest stand in June 2008. All spectral reflectance measurements were taken in the nadir direction under clear sky conditions ~3 cm above sunlit targets (leaves or moss/lichen layer and ground). No fore-optics was used. The measurements were standardized to reflectance using a Spectralon diffuse reflectance target (Labsphere Inc., North Sutton, NH, USA). The average HDRF was obtained based on the reflectance of the cover types weighted by their area fractions as derived from photos taken at the site.

The understory spectra at Hyytiälä [*Rautiainen et al.*, 2011], Järvselja [*Nikopensius et al.*, 2015], and Yatir sites were obtained following the protocol of *Rautiainen et al.* [2011]. The understory spectra were measured under diffuse light conditions with fiber input supplied ASD FieldSpec Pro spectrometer, covering 350–1050 nm region. The sampling interval was 1.4 nm with the resolution 3 nm at full width at half maximum at 700 nm. All measurements were taken when the Sun was completely blocked by the clouds, or direct solar radiance was totally attenuated by the long path length in tree crown layer at low solar elevations close to sunset. The understory spectra were measured along respective transects across each stand, resulting in 40–50 measurement points (with three understory spectra per each measurement point) per transect. Three spectra above a Spectralon white panel were recorded at the beginning and end of each transect and also along it after every four understory spectra measurement points.

Spectral measurements were then processed to correspond to HDRFs. Two Spectralon reflectance measurements made before and after each understory spectrum quadruplet along given transect were interpolated linearly in time to estimate the spectral irradiance for the moments when the understory spectra were recorded. A hemispherical-conical reflectance factor was obtained with an "uncalibrated" Spectralon reflectance spectrum and the interpolated irradiance.

ASD FieldSpec Pro measurements were performed under fully illuminated conditions at Laegern in September 2011 [*Schneider et al.*, 2014]. The objects were placed and measured in full sunshine on a fully absorbing background (black cloth). The average HDRF background signal was estimated by linear mixing of the percentages of understory vegetation coverage (>3 m, 5%; 0–3 m, 32%), unvegetated areas (18%), and litter (45%).

At Gwangneung site, light-emitting diode (LED) sensors were installed at four canopy depths using a flux tower structure [*Ryu et al.*, 2014]. LED sensors as spectrally selective light detector were reported and tested

in a previous study [*Ryu et al.*, 2010]. LEDs in the sensor heads were housed beneath Teflon (Teflon®, DuPont, Wilmington, DE, USA) to diffuse the incoming light at Gwangneung. One sensor head was directed to the zenith and the other toward the nadir direction, which enabled monitoring bihemispheric reflectance. We assembled four-band (red, green, blue, and near-infrared (NIR)) LED sensors and used red and NIR channels to compute NDVI. As overstory canopy was distinct above 12 m height [*Song and Ryu*, 2015], we used LED sensors data collected at 12 m height to retrieve understory NDVI. CR1000 data loggers (Campbell Sci., Inc., CSI, Logan, UT, USA) sampled irradiance from each spectral channel every 30 s and stored half-hour mean values throughout the growing season in 2013. Series of concurrent LED measurement- and ASD measurement-based NDVI values showed good agreement in the fall 2015 (results not shown).

A relative spectral response function used to simulate Moderate Resolution Imaging Spectroradiometer (MODIS) data from in situ spectrometer measurements was used to compute broadband HDRFs for red (620–670 nm) and NIR (841–876 nm) wavelengths at each site. Finally, a broadband normalized difference vegetation index (NDVI) [*Rouse et al.*, 1973] was calculated from these red and NIR bands. The variability in the understory NDVI due to the spatial heterogeneity of understory vegetation differed between sites. The rather infertile sites (e.g., Järvselja RAMI pine; Yatir) had lower variability in field measurements (standard deviation (SD) ~ 0.06), while more fertile sites (e.g., Järvselja RAMI birch) had higher variability (SD ~ 0.13).

2.3. MODIS Data

The MODIS BRDF/albedo product (MCD43A1, version 5) [*Lucht et al.*, 2000; *Schaaf et al.*, 2002] is a MODIS standard product that provides the weighting parameters associated with the RossThick-LiSparse BRDF model that describes the reflectance anisotropy at 500 m resolution. The BRDF parameters are produced every 8 days with 16 days of acquisition using both Terra and Aqua data [*Schaaf et al.*, 2002]. We retrieved the forest understory signal using the BRDF model parameters (isotropic, volumetric, and geometric kernel weights) [*Roujean et al.*, 1992] for MODIS band 1 (red, 620–670 nm) and band 2 (NIR, 841–876 nm). MODIS data used in this study were acquired for tiles covering the test sites and years with available in situ measurements described in section 2.1. For each date, we reconstructed the bidirectional reflectance factor (BRF) values for required geometries (see section 3). All the MCD43A1 data were downloaded from the Data Pool of Land Processes Distributed Active Archive Center. The associated data quality (MCD43A2) product was also downloaded from the same source and was used to analyze the effect of retrieval quality on the accuracy of calculating understory reflectance.

3. Retrieval Method

The total top-of-canopy reflectance (R) can be expressed as a linear combination of the contributions from the sunlit and viewed and shaded and viewed components [*Li and Strahler*, 1985; *Chen et al.*, 2000; *Bacour and Bréon*, 2005; *Chopping et al.*, 2008]:

$$R = R_T \cdot k_T + R_G \cdot k_G + R_{ZT} \cdot k_{ZT} + R_{ZG} \cdot k_{ZG} \qquad (1)$$

where R_T, R_G, R_{ZT}, and R_{ZG} are the reflectance factors of the sunlit crowns, sunlit understory, shaded crowns, and shaded understory, respectively. R_G can be considered the BRF of the target (understory). The k_j is the proportions of these components at the chosen view angle or in the instantaneous field of view (IFOV) of the sensor at given irradiation geometry. Based on the assumption that the reflectance factors of the overstory and the understory at the given illumination geometry differ little between chosen view angles, one can derive the understory reflectance factor (R_G) [*Canisius and Chen*, 2007]. *Pisek et al.* [2015a] recently identified the most suitable viewing configuration for the R_G retrieval using a new high angular resolution BRF data set of *Kuusk et al.* [2014] with accompanying in situ measurements of understory reflectance [*Kuusk et al.*, 2013]. Following *Pisek et al.* [2015a], the reflectance at nadir (R_n; view zenith angle (VZA) = 0°) and another zenith angle (R_a; VZA = 40°) with solar zenith angle corresponding to the Sun's position at 10:00 local time for given day and relative azimuth angle (PHI = 130°) can be expressed by equations (2) and (3):

$$R_n = R_T \cdot k_{Tn} + R_G \cdot k_{Gn} + R_{ZT} \cdot k_{ZTn} + R_{ZG} \cdot k_{ZGn} \qquad (2)$$

$$R_a = R_T \cdot k_{Ta} + R_G \cdot k_{Ga} + R_{ZT} \cdot k_{ZTa} + R_{ZG} \cdot k_{ZGa} \qquad (3)$$

The reflectance of shaded tree crowns (R_{ZT}) and understory (R_{ZG}) can be expressed dynamically as functions of their sunlit fractions and the multiple scattering factor M [*White et al.*, 2001, 2002], giving $R_{ZT} = M \cdot R_T$ and

Table 3. Stand Parameters for the Four-Scale Model

Stand	Deciduous	Coniferous
Stand density (trees/ha)	500,1000,2000	500,1000,2000
Tree height (m)	25	16
Length of live crown (m)	9.2	4.2
Radius of crown projection (m)	1.87	1.5
Leaf area index (m^2/m^2)	1,2,3	1,2,3

$R_{ZG} = M \cdot R_G$, where $M = R_Z/R$ for a reference target. M is predetermined by the four-scale geometric-optical model inversion [*Chen and Leblanc*, 1997]. The proportions of the components (k_j) for each stand were retrieved with the four-scale model [*Chen and Leblanc*, 1997] using parameters for generalized deciduous and coniferous tree stands (see Table 3) common to European boreal/hemiboreal zone [*Kuusk et al.*, 2013; *Crowther et al.*, 2015]. Combining and solving equations (2) and (3) and inserting the MODIS-derived R_n and R_a, the understory reflectance R_G for red and NIR band and the resulting understory NDVI ($NDVI_u$) value can be calculated. For the general retrieval of understory signal over large areas, the input stand parameters from Table 2 may not be always precisely known. *Gemmell* [2000] also found that specifying the correct range/constraints for understory alone greatly reduced the errors in the retrieved overstory parameters [*Gemmell*, 2000]. Following *Gemmell* [2000], we opted for reporting a general range of understory NDVI values using the combinations of parameter values from Table 3 for each site and date.

4. Results

The retrieval method was able to track seasonal dynamics of understory over a very wide NDVI range (Figure 1). The PFRR site has the smallest overstory effective leaf area index ($LAI_e = 0.62$) [*Kobayashi et al.*, 2014], the understory is well exposed, and the retrieved understory NDVI range aligns well with the in situ measurements at day of year (DOY) 188 (Figure 1a). The high understory visibility with a weak seasonality of overstory LAI throughout the growing season [*Yang et al.*, 2014] translates into a rather narrow range and lower uncertainty of understory NDVI values.

Black spruce also dominates overstory in Sudbury, but the site is more fertile and the measured in situ understory NDVI value (0.76) is higher than in PFRR. The canopy is rather closed and prevents a correct retrieval of understory NDVI dynamics at 500 m spatial resolution (Figure 1b).

The site fertility is well reflected in the seasonal variation of understory NDVI measurements of the southern boreal and semiboreal forest sites as well (Figures 1c–1f). The fertile sites both in Hyytiälä (Figure 1c) and Järvselja (Figure 1e) experience a rapid understory NDVI increase at the beginning of the season, followed by a clear understory NDVI decrease in the fall. There is also a visible shift in the earlier development of understory in the more southern RAMI birch site in Järvselja (Figure 1e) compared to the similar stand in Hyytiälä (Figure 1c) that is observed both by in situ and satellite data. The less fertile sites (Figures 1d and 1f) showed progressively smaller variations with a more gradual increase in understory NDVI and not very pronounced signs of senescence. Importantly, results from the European boreal forests (Figures 1c–1f) confirm that the retrieval method is indeed capable of tracking the actual understory NDVI dynamics throughout the whole growing season. *Rautiainen et al.* [2011] previously noted that the understory and tree canopy layers develop at a similar pace in the spring in boreal Hyytiälä. *Nikopensius et al.* [2015] illustrated that in the case of the fertile sites in more southern semiboreal forests of Järvselja, there is a clear early understory development prior to canopy development due to the presence of spring ephemerals. However, it should be noted that such mismatch in the seasonal development of understory and tree canopy layers might not be always detectable while using NDVI from satellite images as the indicator [*Rautiainen et al.*, 2011].

The seasonal trajectory of understory NDVI reflects the longer growing season in the temperate forests at Laegern (Figure 1g) and Gwangneung (Figure 1h). At the same time, there is a clear mismatch between the retrieved range of understory NDVI values and available in situ measurements at Laegern. Laegern has a closed canopy with LAI_e up to 5.5 and very big trees ($h > 30$ m; max. crown radius > 10 m; Table 1). The dense and closed canopy obscures understory especially at off-nadir angles [*Rautiainen et al.*, 2009]. Figure 1g shows that under such circumstances the correct independent estimation of understory signal is not possible. Gwangneung (Figure 1h) has sparser, more open canopy and smaller trees ($h = 18$ m; Table 1) relative to Laegern, and the understory NDVI values are aligned with in situ measurements much better than in case of Laegern.

Yatir is a semiarid plantation with well-visible ground. The distinct understory phenology (disappearance of understory vegetation after March) is properly reflected in the trajectory of understory NDVI retrieved with
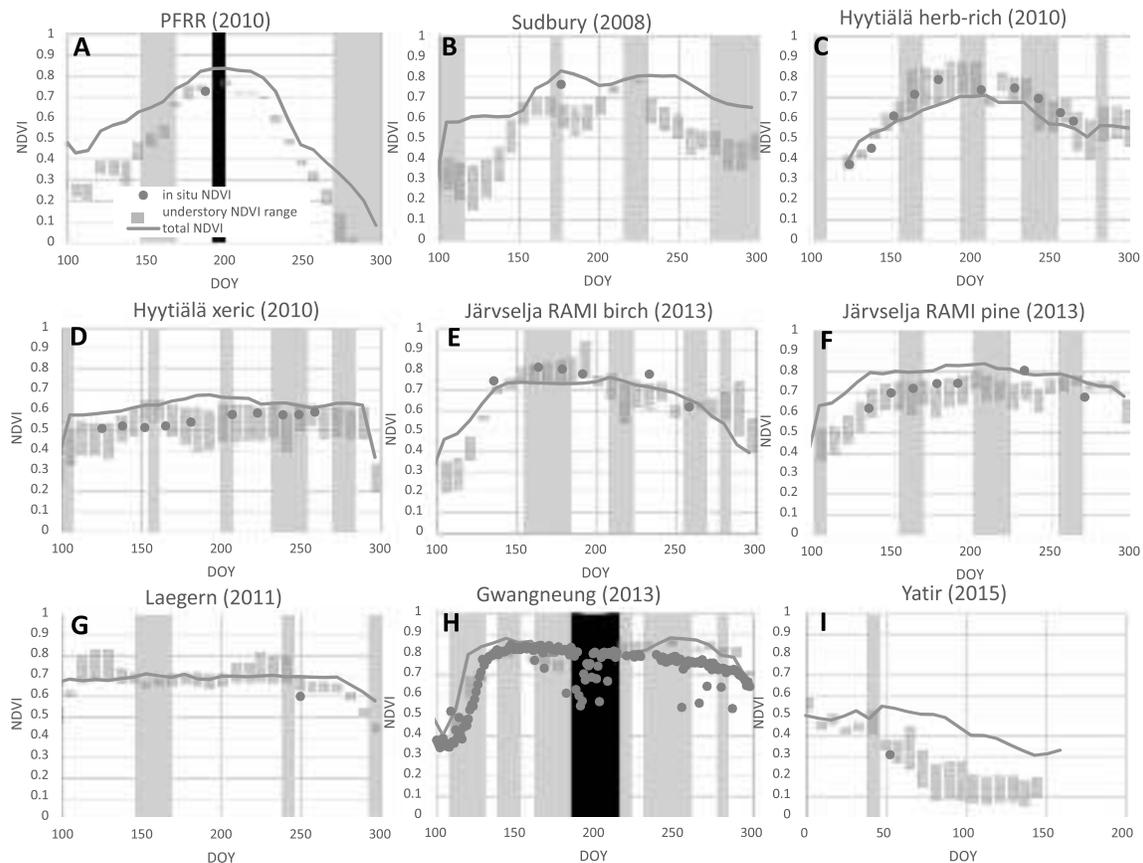
Figure 1. Seasonal profiles of understory NDVI (NDVI$_u$) ranges (blue bars) and their comparison with in situ measurements (purple dots) and computed nadir NDVI values from MODIS BRDF/albedo data (green lines). Gray bars indicate MODIS BRDF parameters with lower quality flags; black bar indicates no data available. (For interpretation of the references to color in this figure legend, the reader is referred to the web version of this article.)

the satellite data (Figure 1i). The measured in situ value at DOY 54 in 2015 (0.29) also falls well within the estimated understory NDVI range from MODIS.

The obtained results allow better understanding of limitations of the retrieval method over the wide range of forest types. Understory signal retrieval is possible in sparse and clumped canopies, where the scattering within the tree crowns and from understory is likely to be predominantly volumetric. The influence of understory signal cannot be neglected under such circumstances. The retrieval method showed its capabilities over a wide range of understory NDVI values and its effectiveness in tracking the seasonal dynamics irrespective of the timing of the main growing period.

The retrieval method was originally proposed for a boreal forest, and yet our results indicate that it may well perform outside this forest type as well, given the understory is visible at the required off-nadir angle configuration (VZA = 40°; PHI = 130°). Importantly, in agreement with simulations by *Pisek et al.* [2010], the performance of the method was shown not to be critically sensitive to the assumed stand density in case of low to intermediate densities, when the influence of the background reflectance on the total canopy signal is the greatest [*Rautiainen et al.*, 2007].

The performance of the method is severely limited in rather closed canopies such as Sudbury or Laegern. The dominant scattering effect is geometric-optic (shadowing) in such stands. There is only a negligible understory influence on the top-of-canopy signal. The understory signal retrieval is then not independently possible. At the same time, under such circumstances the missing information about the understory signal does not hinder the remote sensing of biophysical properties of prime interest—LAI and fraction of absorbed photosynthetically active radiation (fAPAR) of forest canopy layer [*Garrigues et al.*, 2008; *Weiss et al.*, 2014].

5. Conclusions

We report on the performance of physically based approach to estimate understory NDVI from MODIS BRDF/albedo data and its seasonal dynamics over a wide range of forest types. Our results indicate that the retrieval method performs well over different types of open forests. We also demonstrate the limitations of the method, particularly in closed canopies, where the understory signal retrieval is not possible independently from the overstory. The retrieval of understory signal can be used, e.g., to improve the estimates of leaf area index (LAI) [*Gonsamo and Chen*, 2014], fAPAR in sparsely vegetated areas [*Weiss et al.*, 2014], and also to study the phenology of understory layer [*Richardson and O'Keefe*, 2009]. Our results are particularly useful to producing Northern Hemisphere maps of seasonal dynamics of forests [*Park et al.*, 2015], allowing to separately retrieve understory variability, being a main contributor to spring emergence and fall senescence uncertainty [*Garonna et al.*, 2014]. The inclusion of understory variability in ecological models will ultimately improve prediction and forecast horizons [*Petchey et al.*, 2015] of vegetation dynamics.

References

Bacour, C., and F. M. Bréon (2005), Variability of biome reflectance directional signatures as seen by POLDER, *Remote Sens. Environ.*, *98*, 80–95.

Canisius, F., and J. M. Chen (2007), Retrieving forest background reflectance in a boreal region from Multi-angle Imaging SpectroRadiometer (MISR) data, *Remote Sens. Environ.*, *107*(1–2), 312–321.

Chapin, F. S. (1983), Nitrogen and phosphorous nutrition and nutrient cycling by evergreen and deciduous understory shrubs in an Alaskan black spruce forest, *Can. J. For. Res.*, *13*, 773–781.

Chastain, R. A., W. S. Currie, and P. A. Townsend (2006), Carbon sequestration and nutrient cycling implications of the evergreen understory layer in Appalachian forests, *For. Ecol. Manage.*, *231*, 63–77.

Chen, J. M., and S. G. Leblanc (1997), A four-scale bidirectional reflectance model based on canopy architecture, *IEEE Trans. Geosci. Remote Sens.*, *35*(5), 1316–1337.

Chen, J. M., X. Li, T. Nilson, and A. Strahler (2000), Recent advances in geometrical optical modelling and its applications, *Remote Sens. Rev.*, *18*(2-4), 227–262.

Chopping, M., G. G. Moisen, L. H. Su, A. Laliberte, A. Rango, J. V. Martonchik, and D. P. C. Peters (2008), Large area mapping of southwestern crown cover, canopy height, and biomass using the NASA Multiangle Imaging Spectro-Radiometer, *Remote Sens. Environ.*, *112*(5), 2051–2063.

Crowther, T. W., et al. (2015), Mapping tree density at a global scale, *Nature*, *525*, 201–205.

D'Amato, A. W., D. A. Orwig, and D. R. Foster (2009), Understory vegetation in old-growth and second-growth *Tsuga canadensis* forests in western Massachusetts, *For. Ecol. Manage.*, *257*, 1043–1052.

D'odorico, P., A. Gonsamo, B. Pinty, N. Gobron, N. Coops, E. Mendez, and M. E. Schaepman (2014), Intercomparison of fraction of absorbed photosynthetically active radiation products derived from satellite data over Europe, *Remote Sens. Environ.*, *142*, 141–154.

Eugster, W., K. Zeyer, M. Zeeman, P. Michna, A. Zingg, N. Buchmann, and L. Emmenegger (2007), Methodical study of nitrous oxide eddy covariance measurements using quantum cascade laser spectrometry over a Swiss forest, *Biogeosciences*, 927–939.

Garonna, I., R. de Jong, A. J. de Wit, C. A. Mucher, B. Schmid, and M. E. Schaepman (2014), Strong contribution of autumn phenology to changes in satellite-derived growing season length estimates across Europe (1982–2011), *Global Change Biol.*, *20*, 3457–3470.

Garrigues, S., et al. (2008), Validation and intercomparison of global leaf area index products derived from remote sensing data, *J. Geophys. Res.*, *113*, G02028, doi:10.1029/2007JG000635.

Gemmell, F. (2000), Testing the utility of multi-angle spectral data for reducing the effects of background spectral variations in forest reflectance model inversion, *Remote Sens. Environ.*, *72*, 46–63.

Gilliam, F. S., and M. R. Roberts (2003), *The Herbaceous Understory in Forests of Eastern North America*, 464 pp., Oxford Univ. Press, New York.

Gonsamo, A., and J. M. Chen (2014), Improved LAI algorithm implementation to MODIS data by incorporating background, topography and foliage clumping information, *IEEE Trans. Geosci. Remote Sens.*, *52*, 1076–1088.

Grünzweig, J. M., T. Lin, A. Schwartz, and D. Yakir (2003), Carbon sequestration in arid-land forest, *Global Change Biol.*, *9*(5), 791–799.

Jiao, T., R. Liu, Y. Liu, J. Pisek, and J. M. Chen (2014), Mapping global seasonal forest background reflectivity with multi-angle imaging spectroradiometer data, *J. Geophys. Res. Biogeosci.*, *119*, doi:10.1002/2013JG002493.

Hart, S. A., and H. Y. H. Chen (2006), Understory vegetation dynamics of North American boreal forests, *Crit. Rev. Plant Sci.*, *25*, 381–397.

Kobayashi, H., R. Suzuki, and S. Kobayashi (2007), Reflectance seasonality and its relation to the canopy leaf area index in an eastern Siberian larch forest: Multi-satellite data and radiative transfer analyses, *Remote Sens. Environ.*, *106*, 238–252.

Kobayashi, H., R. Suzuki, S. Nagai, T. Nakai, and Y. Kim (2014), Spatial scale and landscape heterogeneity effects on FAPAR in an open canopy black spruce forest in interior Alaska, *IEEE Geosci. Remote Sens. Lett.*, *11*(2), 564–568, doi:10.1109/LGRS.2013.2278426.

Koizumi, H., and Y. Oshima (1985), Seasonal changes in photosynthesis of four understory herbs in deciduous forests, *Bot. Mag. Tokyo*, *98*, 1–13.

Kuusk, A., M. Lang, and J. Kuusk (2013), Database of optical and structural data for the validation of forest radiative transfer models, in *Radiative Transfer and Optical Properties of Atmosphere and Underlying Surface*, *Light Scattering Rev.*, vol. 7, edited by A. A. Kokhanovsky, pp. 109–148, Springer, Berlin.

Kuusk, A., J. Kuusk, and M. Lang (2014), Measured spectral bidirectional reflection properties of three mature hemiboreal forests, *Agric. For. Meteorol.*, *185*, 14–19.

Leiterer, R., R. Furrer, M. E. Schaepman, and F. Morsdorf (2015), Forest canopy-structure characterization: A data-driven approach, *For. Ecol. Manage.*, *358*, 48–61.

Li, X. W., and A. H. Strahler (1985), Geometric-optical modeling of a conifer forest canopy, *IEEE Trans. Geosci. Remote Sens.*, *23*(5), 705–721.

Lucht, W., C. B. Schaaf, and A. H. Strahler (2000), An algorithm for the retrieval of albedo from space using semiempirical BRDF models, *IEEE Trans. Geosci. Remote Sens.*, *38*, 977–998.

Lukeš, P., P. Stenberg, and M. Rautiainen (2013), Relationship between forest density and albedo in the boreal zone, *Ecol. Modell.*, *261-262*, 74–79.

Maseyk, K. S., T. Lin, E. Rotenberg, J. M. Grünzweig, A. Schwartz, and D. Yakir (2008), Physiology-phenology interactions in a productive semi-arid pine forest, *New Phytol.*, *178*(3), 603–616, doi:10.1111/j.1469-8137.2008.02391.x.

Miller, J., et al. (1997), Seasonal change in the understory reflectance of boreal forests and influence on canopy vegetation indices, *J. Geophys. Res.*, *102*(D24), 29,475–29,482, doi:10.1029/97JD02558.

Nikopensius, M., J. Pisek, and K. Raabe (2015), Spectral reflectance patterns and seasonal dynamics of common understory types in three mature hemi-boreal forests, *Int. J. Appl. Earth Observ. Geoinf.*, *43*, 84–91.

Nilsson, M.-C., and D. A. Wardle (2005), Understory vegetation as a forest ecosystem driver: Evidence from the northern Swedish boreal forest, *Front. Ecol.*, *3*, 421–428.

Nyland, R. D., A. L. Bashant, K. K. Bohn, and J. M. Verostek (2006), Interference to hardwood regeneration in northeastern North America: Controlling effects of American beech, striped maple, and hobblebush, *Northern J. Appl. For.*, *23*, 122–132.

Park, H., S.-J. Jeong, C.-H. Ho, J. Kim, M. E. Brown, and M. E. Schaepman (2015), Nonlinear response of vegetation green-up to local temperature variations in temperate and boreal forests in the Northern Hemisphere, *Remote Sens. Environ.*, *165*, 100–108.

Peltoniemi, J., S. Kaasalainen, J. Näränen, M. Rautiainen, P. Stenberg, H. Smolander, S. Smolander, and P. Voipio (2005), BRDF measurement of understory vegetation in pine forests: Dwarf shrubs, lichen and moss, *Remote Sens. Environ.*, *94*, 343–354.

Petchey, O. L., et al. (2015), The ecological forecast horizon, and examples of its uses and determinants, *Ecol. Lett.*, *17*, 597–611.

Pinty, B., T. Lavergne, T. Kaminski, O. Aussedat, R. Giering, N. Gobron, M. Taberner, M. M. Verstraete, M. Voßbeck, and J.-L. Widlowski (2008), Partitioning the solar radiant fluxes in forest canopies in the presence of snow, *J. Geophys. Res.*, *113* D04104, doi:10.1029/2007JD009096D04104.

Pisek, J., and J. M. Chen (2009), Mapping forest background reflectivity over North America with multi-angle imaging spectroradiometer (MISR) data, *Remote Sens. Environ.*, *113*, 2412–2423.

Pisek, J., J. M. Chen, J. Miller, J. Freemantle, J. Peltoniemi, and A. Simic (2010), Mapping forest background in a boreal region using multiangle Compact Airborne Spectrographic Imager data, *IEEE Trans. Geosci. Remote Sens.*, *48*(1), 499–510.

Pisek, J., M. Rautiainen, J. Heiskanen, and M. Mõttus (2012), On the retrieval of seasonal dynamics of forest understory reflectance in a Northern European boreal forest from MODIS BRDF data, *Remote Sens. Environ.*, *17*, 464–468.

Pisek, J., M. Lang, and J. Kuusk (2015a), A note on suitable viewing configuration for retrieval of forest understory reflectance from multi-angle remote sensing data, *Remote Sens. Environ.*, *156*, 242–246.

Pisek, J., M. Rautiainen, M. Nikopensius, and K. Raabe (2015b), Estimation of seasonal dynamics of understory NDVI in northern forests using MODIS BRDF data: Semi-empirical versus physically-based approach, *Remote Sens. Environ.*, *163*, 42–47.

Rautiainen, M., and J. Heiskanen (2013), Seasonal contribution of understory vegetation to reflectance of a boreal landscape at different spatial scales, *IEEE Geosci. Remote Sens. Lett.*, *10*, doi:10.1109/LGRS.2013.2247560.

Rautiainen, M., J. Suomalainen, M. Mõttus, P. Stenberg, P. Voipio, J. Peltoniemi, and T. Manninen (2007), Coupling forest canopy and understory reflectance in the Arctic latitudes of Finland, *Remote Sens. Environ.*, *110*, 332–343.

Rautiainen, M., T. Nilson, and T. Lükk (2009), Seasonal reflectance trends of hemiboreal birch forests, *Remote Sens. Environ.*, *113*, 805–815.

Rautiainen, M., M. Mõttus, J. Heiskanen, A. Akujärvi, T. Majasalmi, and P. Stenberg (2011), Seasonal reflectance dynamics of common understory types in a Northern European boreal forest, *Remote Sens. Environ.*, *115*, 3020–3028.

Richardson, A. D., and J. O'Keefe (2009), Phenological differences between understory and overstory, in *Phenology of Ecosystem Processes*, pp. 87–117, Springer, New York.

Roujean, J. -L., M. Leroy, and P. Y. Deschamps (1992), A bi-directional reflectance model of the Earth's surface for the correction of remote sensing data, *J. Geophys. Res.*, *97*(D18), 20,455–20,468, doi:10.1029/92JD01411.

Rouse, W. J., H. R. Haas Jr., A. J. Schell, and W. D. Deering (1973), Monitoring vegetation systems in the Great Plains with ERTS, in *Third ERTS Symposium*, *NASASP-351*, vol. I, pp. 309–317, NASA, Washington, D. C.

Ryu, Y., D. D. Baldocchi, J. Verfaillie, S. Ma, M. Falk, I. Ruiz-Mercado, T. Hehn, and O. Sonnentag (2010), Testing the performance of a novel spectral reflectance sensor, built with light emitting diodes (LEDs), to monitor ecosystem metabolism, structure and function, *Agric. For. Meteorol.*, *150*, 1597–1606.

Ryu, Y., G. Lee, S. Jeon, Y. Song, and H. Kimm (2014), Monitoring multi-layer canopy spring phenology of temperate deciduous and evergreen forests using low-cost spectral sensors, *Remote Sens. Environ.*, *149*, 227–238.

Schaaf, C. B., et al. (2002), First operational BRDF albedo, nadir reflectance products from MODIS, *Remote Sens. Environ.*, *83*, 135–148.

Schaepman, M. E., S. L. Ustin, A. J. Plaza, T. H. Painter, J. Verrelst, and S. Liang (2009), Earth system science related imaging spectroscopy-An assessment, *Remote Sens. Environ.*, *113*, S123–S137.

Schaepman-Strub, G., M. E. Schaepman, T. H. Painter, S. Dangel, and J. V. Martonchik (2006), Reflectance quantities in optical remote sensing—Definitions and case studies, *Remote Sens. Environ.*, *103*, 27–42.

Schneider, F. D., R. Leiterer, F. Morsdorf, J.-P. Gastellu-Etchegorry, N. Lauret, N. Pfeifer, and M. E. Schaepman (2014), Simulating imaging spectrometer data: 3D forest modeling based on LiDAR and in situ data, *Remote Sens. Environ.*, *152*, 235–250.

Song, Y., and Y. Ryu (2015), Seasonal changes in vertical canopy structure in a temperate broadleaved forest in Korea, *Ecol. Res.*, *30*, 821–831.

Sprintsin, M., S. Cohen, K. Maseyk, E. Rotenberg, J. Grunzweig, A. Karnieli, et al. (2011), Long term and seasonal courses of leaf area index in a semi-arid forest plantation, *Agric. For. Meteorol.*, *151*, 565–574.

Suzuki, R., H. Kobayashi, N. Delbart, J. Asanuma, and T. Hiyama (2011), NDVI responses to the forest canopy and floor from spring to summer observed by airborne spectrometer in eastern Siberia, *Remote Sens. Environ.*, *115*, 3615–3624.

Weiss, M., et al. (2014), On line validation exercise (OLIVE): A web based service for the validation of medium resolution land products. Application to FAPAR products, *Remote Sens.*, *6*, 4190–4216.

White, P. H., J. R. Miller, and J. M. Chen (2001), Four-scale linear model for anisotropic reflectance (FLAIR) for plant canopies—Part I: Model description and partial validation, *IEEE Trans. Geosci. Remote Sens.*, *39*, 1073–1083.

White, P. H., J. Deguise, J. Schwartz, R. Hitchcock, and K. Staenz (2002), Defining shaded spectra by model inversion for spectral unmixing of hyperspectral datasets—Theory and preliminary application, in *Proceedings of the International Geoscience And Remote Sensing Symposium (IGARSS) and 24th Canadian Symposium on Remote Sensing*, pp. 989–991, IEEE, Toronto, Canada.

Widlowski, J. L., et al. (2007), Third radiation transfer model intercomparison (RAMI) exercise: Documenting progress in canopy reflectance models, *J. Geophys. Res.*, *112*, D09111, doi:10.1029/2006JD007821.

Yang, W., H. Kobayashi, R. Suzuki, and K. Nasahara (2014), A simple method for retrieving understory NDVI in sparse needleleaf forests in Alaska using MODIS BRDF data, *Remote Sens.*, *6*, 11,936–11,955.